On heavy carbon doping of MgB$_2$

Deepa Kasinathan, K.-W. Lee, W.E. Pickett *

Department of Physics, University of California, Davis CA 95616, USA

Abstract

Heavy carbon doping of MgB$_2$ is studied by first principles electronic structure studies of two types, an ordered supercell (Mg(B$_{1-x}$C$_x$)$_2$, $x = 0.0833$) and also the coherent potential approximation method that incorporates effects of B–C disorder. For the ordered model, the twofold degenerate σ-bands that are the basis of the high temperature superconductivity are split by 60 meV (i.e. 7 meV/% C) and the σ Fermi cylinders contain 0.070 holes/cell, compared to 0.11 for MgB$_2$. A virtual crystal treatment tends to overestimate the rate at which σ holes are filled by substitutional carbon. The coherent potential approximation (CPA) calculations give the same rate of band filling as the supercell method. The occupied local density of states of C is almost identical to that of B in the upper 2 eV of the valence bands, but in the range -8 eV to -2 eV, C has a considerably larger density of states. The calculations indicate that the σ Fermi surface cylinders pinch off at the zone center only above the maximum C concentration $x \approx 0.10$. These results indicate that Mg(B$_{1-x}$C$_x$)$_2$ as well as Mg$_{1-x}$Al$_x$B$_2$ is a good system in which to study the evolution of the unusual electron–phonon coupling character and strength as the crucial σ hole states are filled.

1. Introduction

Discovery of superconductivity at $T_c \approx 40$ K in MgB$_2$ has enlivened not only interest in new classes of superconductors with high T_c and novel two-gap behavior, but also pursuit of new materials for applications that require high critical current densities and high critical fields (H_{c2}). In highly resistive films (due to unreacted components and/or oxygen and carbon impurities) the perpendicular and parallel critical fields have reached [1] $H_{c2}^{\perp} \approx 34$ T, $H_{c2}^{\parallel} \approx 49$ T, making MgB$_2$ a real possibility for a high field conductor. Such application require defects or grain boundaries to pin the vortices whose motion would otherwise lead to energy dissipation and joule heating. Such defects also affect the underlying electronic structure and pairing interaction, at least in some parts of the sample, and often decrease T_c. The simplest defect to understand is the substitutional impurity, which provides a

* Corresponding author. Tel.: +1 530 7534123; fax: +1 530 7524717.

E-mail address: pickett@physics.ucdavis.edu (W.E. Pickett).

means of varying the intrinsic properties in a continuous and controllable manner and may enhance pinning mechanisms. Although readily synthesizable as a stoichiometric, rather clean compound, the MgB_2 lattice resists most attempts to alloy, both on the Mg and B sites, at more than the very dilute level.

The two established exceptions are Al substitution for Mg, and C substitution for B, both of which lead to a rapid decrease in T_c. Published reports on the behavior vary considerably with synthesis method and sample treatment, but some of the general behavior seems to be established. Al substitution should be the simpler one, since the very strongly bonded honeycomb structure B layers remain intact, and simple rigid band filling of the hole states at first appears to be a likely possibility. Up to $y = 0.10$ in $Mg_{1-y}Al_yB_2$ that appears to be the case, with T_c decreasing smoothly. Beyond the concentration $y = 0.10$, however, there are signs of two-phase behavior (two c lattice parameters in diffraction studies) arise [2]. Around $y = 0.25$ the system reverts to a single phase very low and finally vanishing T_c. A study of the trends in electron–phonon coupling strength using first principles calculations in the virtual crystal approximation [3] reported a sharp change of behavior at $y = 0.25$. A thorough study of the energetics of Al substitution revealed a strong tendency for superstructure formation [4] at $y = 0.25$ (and $y = 0.75$). Still, the observed onset of two-phase behavior already at $y = 0.10$ is unexplained, and nonstoichiometry [5] and microscopic defects must be kept in mind.

Unlike the Al alloying case where there has been at least rough consensus on changes of properties, reports of the change in T_c and structure with addition of carbon on MgB_2 have varied widely. These differences seem in some cases to reflect real differences in materials due to the various methods of synthesis and heat treatment, and the samples prepared were highly mixed phase, thereby creating additional uncertainty. The very similar X-ray scattering strength of the B and C atoms has rendered standard X-ray diffraction ineffective in determining the C content of a sample. Reports early on suggested C miscibilities in $Mg(B_{1-x}C_x)_2$ as small [6] as $x = 0.02$ to as large [7] as $x = 0.3$. Recent studies of several groups suggest that $x = 0.2$ can be achieved while larger concentrations are questionable [8–10] although reports of larger C concentrations under high pressure growth persist [11].

With some of the materials questions coming under control, the observation trends are raising some serious questions. The decrease in T_c follows $dT_c/dx \sim 1$ K/% C [12], with several reports of $T_c \approx 21$–23 K at $x = 0.2$ [8–10]. However, with carbon adding one electron and the σ-bands of MgB_2 holding only ~ 0.11 holes per unit cell [13], one might guess that the σ-bands would be filled (or nearly so, as the π-bands can also accept carriers) and superconductivity would have vanished. Not only is T_c still robust at $x = 0.2$, analysis of tunneling spectra indicates two-band superconductivity is retained [14,15], whereas it might also seem likely that disorder scattering should have averaged out the gap to a single value. The upper critical field H_{c2} initially increases strongly with C content as T_c is depressed, reaching a maximum [1,12,16] of ~ 33–35 T. This critical field is substantially less than that for more disordered films (see above).

Recent studies seem to agree that C can be introduced substitutionally for B up to 10% replacement $x = 0.10$ [8,17]. Tunneling spectroscopies indicate that $Mg(B_{1-x}C_x)_2$ remains a two-gap superconductor [8,14] (i.e. the gap anisotropy is not washed out by scattering) for $10 \pm 2\%$ C substitution for B. This question of how the anisotropy gets washed out has attracted much interest. Similarly, the mechanisms underlying the high critical fields are not understood. These questions are not the focus of the present study, although the knowledge gained from first principles calculations will be useful in the resolution of these topics.

A few first principles calculations have been done for C substitution of B in MgB_2. Pseudopotential calculations including relaxation in a 27 unit cell supercell [18] confirmed that substitutional C is energetically favorable to interstitial C, and that the C–B bond length is 5–6% shorter than the bulk B–B bond length. A projector-augmented-wave calculation [19] reported a smaller relaxation, but the difference may be due to con-

136 straints related to supercell size. A coherent poten-
137 tial approximation study of the disordered alloy
138 using a Korringa–Kohn–Rostoker multiple scat-
139 tering method in the atomic sphere approximation
140 [20] revealed relatively small effects of disorder in
141 the range $0 \leqslant x \leqslant 0.3$. The main effect of C substi-
142 tution was reported to be the raising of the Fermi
143 energy due to the additional carriers, but the filling
144 of the crucial σ hole band was not quantified.
145   In this paper, we present a more detailed analy-
146 sis of the changes in electronic structure, and the
147 effective σ-band doping, using both periodic
148 supercells and disordered alloy calculations. Our
149 study lays the groundwork for another issue in
150 the superconductivity of MgB_2 alloys that has re-
151 ceived no direct attention from experimentalists:
152 the effect of decreasing holes on the strength and
153 character of electron–phonon coupling. Theoreti-
154 cal studies [21–23] have predicted the following
155 remarkable changes in doped MgB_2: as the num-
156 ber of holes decreases (hence the Fermi wavevector
157 k_F of the cylindrical σ Fermi surfaces decreases),
158 (1) the substantial downward renormalization of
159 the E_{2g} bond-stretching modes with $Q \leqslant 2k_F$ does
160 not change, (2) the coupling strengths of these al-
161 ready strongly coupled modes increases, and (3)
162 the total coupling strength λ, and hence T_c, re-
163 mains unchanged. This scenario assumes two-
164 dimensionality of the σ-bands which is only
165 approximately true, and neglects the change of
166 electron–phonon matrix elements which should
167 be reasonable. This argument also neglects the fact
168 that the applicability of conventional electron–
169 phonon (Midgal–Eliashberg) theory, already
170 somewhat suspect [24,25] in MgB_2, definitely be-
171 comes inapplicable as the Fermi energy decreases
172 and approaches more closely the bond-stretching
173 mode energy (65 meV). Item (2) definitely portends
174 unusual dynamics related to the B–B stretch
175 modes. We hope the current paper stimulates
176 experimental investigation into these questions.

177 **2. Calculational methods**

178   Two methods of assessing the effects of substi-
179 tutional C in MgB_2 have been used in the work re-
180 ported here. Our ordered impurity calculations

Table 1
Lattice parameter values used in the virtual crystal and supercell calculations

Lattice parameter	Undoped MgB_2 (Å)	10% Doping $MgB_{1.8}C_{0.2}$ [17] (Å)	8.33% Doping $Mg_6B_{11}C$ (Å)
a	3.083	3.053	$3 \times 3.053 = 49.159$
b	3.083	3.053	$2 \times 3.053 = 6.106$
c	3.521	3.525	3.525

have been performed using the full-potential line- 181
arized augmented plane wave code Wien2k [26], 182
applying the generalized gradient approximation 183
[27] to the exchange-correlation potential. The ba- 184
sis set is reduced by using the APW + lo method 185
[28], retaining the accuracy of the LAPW method. 186
RK_{max} was set to 7.00 which is a high quality basis 187
for the s–p electron systems. The Brillouin zone 188
integration for the supercell was carried out using 189
432 k points in the irreducible part of the zone. We 190
have used the experimental results of Avdeev et al. 191
[17] for the lattice parameters of the 8.33% doped 192
supercell and the 10% doped virtual crystal (Table 193
1). 194
    For the disordered (randomly substituted) alloy 195
calculations, we have used the full-potential non- 196
orthogonal local-orbital minimum-basis scheme 197
(FPLO) [29] applied in the coherent potential 198
approximation (CPA) [30]. In the calculations, 199
1152 ($45 \times 45 \times 10$) irreducible k points, and va- 200
lence orbitals 2s2p3s3p3d for Mg and 2s2p3d for 201
B and C, were used. The implementation of the 202
CPA in FPLO relies on the Blackman–Esterling– 203
Berk theory [31] that includes random off-diagonal 204
matrix elements in the local-orbital representation. 205

3. Ordered $Mg(B_{1-x}C_x)_2$, $x = 0.0833$ 206

    Smaller concentrations of ordered C substitu- 207
tion for B require larger supercells. Our choice of 208
supercell was guided by the desire for a small en- 209
ough C concentration to be relevant to address 210
experimental data, yet not so small as to make it 211
difficult to distinguish the effect of C addition or 212
to make the calculations unreasonably tedious. 213
Since interlayer hopping is not an issue we will ad- 214
dress, the supercell will involve enlargement of 215
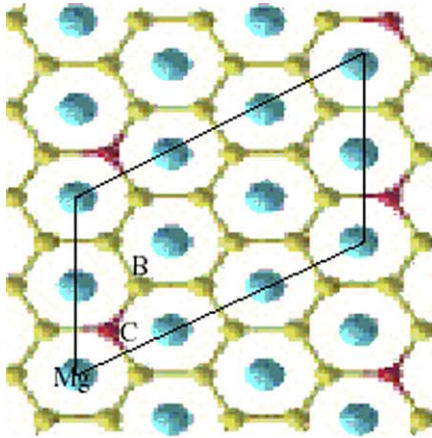
Fig. 1. Top view of the B–C layer of the $Mg_6B_{11}C$ supercell. Large (blue) circles denote Mg atoms, small light (yellow) circles denote boron, and small dark (red) circles denote carbon. The supercell boundary is outlined. (For interpretation of the references in colour in this figure legend, the reader is referred to the web version of this article.)

only a single B layer. The shape of supercell should have as small as possible aspect ratio in order to maximize the separation of C atoms. The compromise we chose was the 8.33% doped supercell $(Mg_6B_{11}C \rightarrow Mg(B_{1-x}C_x)_2, \quad x = 1/12 = 0.0833)$. Fig. 1 shows the top view of the $B_{11}C$ layer in the 2×3 supercell. Each carbon atom has three first, five second, and three third nearest neighbor boron atoms.

3.1. Band structure

There are two effects of carbon substitution: a change in the average potential in the B–C layer, and the breaking of symmetry by C replacement of B in the supercell. In the ordered supercell the potential difference is kept explicit and symmetry breaking will be clear. In Section 6 CPA will be used to probe these effects in a different manner. Another effect, B relaxation around the C impurities, has been addressed previously to some extent, but it will not be studied here since the effect cannot be included within the CPA.

The band structure within 4 eV of the Fermi level (E_F) is shown in Fig. 2. The primary band in the understanding of MgB_2 superconductivity is
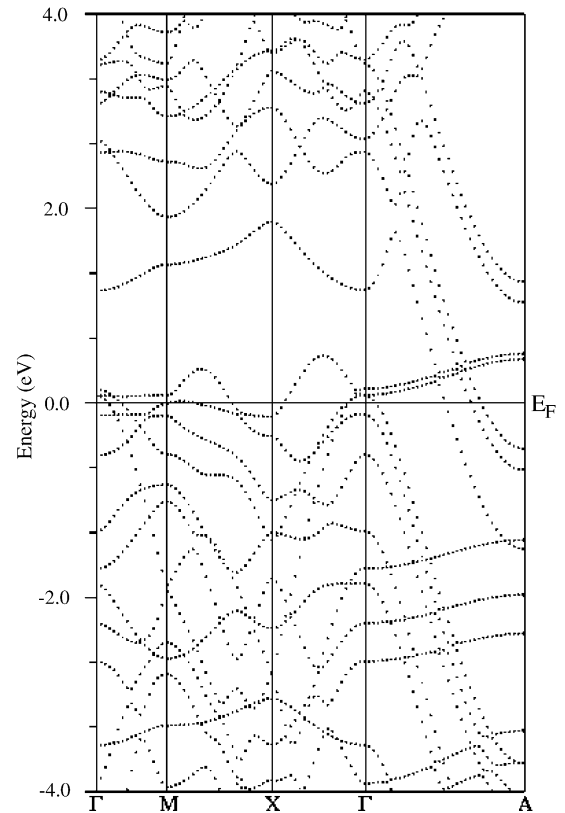
Fig. 2. Band structure of $Mg_6B_{11}C$ in the region of the Fermi level. The twofold degenerate σ-band in the undoped system along the Γ–A is split by 60 meV when 1/12 of B is replaced by C.

the (twofold degenerate) σ-band along the Γ–A direction. The results of supercell band-folding can be distinguished especially for the Γ–A direction, where (for example) the σ-band is replicated at Γ at -1.8 eV, -2.3 eV, -2.6 eV, and even further lower energies.

One of the most readily apparent effects of C doping is the splitting of the σ-bands along Γ–A, by 60 meV. It is helpful in understanding this splitting to obtain the atomic characters of each of the split bands, which will in any case involve only the B and C pσ (p_x, p_y) states. The carbon p contribution is emphasized by enlarged symbols ("fat-bands") in Fig. 3. The lower of the two bands has stronger C content (although this is not easy to distinguish in Fig. 3). In addition, it has more first and second B neighbor character than does
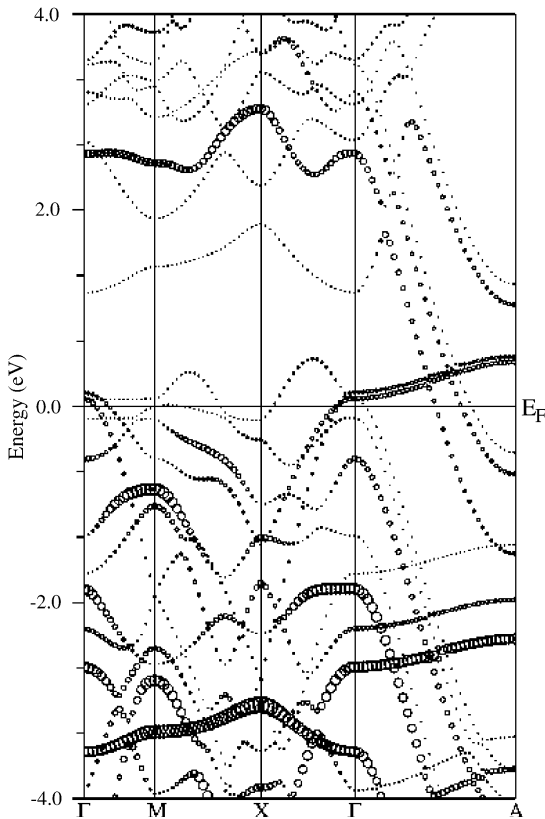
Fig. 3. Bands of $Mg_6B_{11}C$ near the Fermi level, with symbol size proportional to the C 2p character. The σ-bands, split by 60 meV (hardly visible in this figure) lie just above E_F at Γ and disperse upward toward the A point.

Fig. 4. Density of states, total (bottom) and decomposed into B and C contributions on a per-atom basis, for the ordered $x = 1/12$ model. The primary B–C difference is that the C DOS is lower in the -2 eV to E_F region, but higher in the lower region -8 eV to -2 eV.

257 the upper band. The upper band contains more
258 third neighbor B character, this being the B site
259 farthest from the C atom and representative of
260 the bulk material. The interpretation of this split-
261 ting is that lower band has been pulled down due
262 to the stronger potential of the C atom compared
263 to that of B. The 60 meV splitting for $x = 1/12$ pro-
264 vides (assuming a linear effect in this concentration
265 range) an energy scale for σ-band broadening
266 $\gamma_0 \approx 7$ meV/% C content.

267 *3.2. Density of states*

268   Fig. 4 shows the total and atom-projected den-
269 sity of states (DOS) of the 8.33% doped system.
270 The C and B DOS are similar at and above E_F,
271 but the C DOS is somewhat lower in the interval

272 within 2 eV below E_F. The C DOS is larger than
273 that of B in the -8 eV to -3 eV region. Based
274 on charge within spheres of 1.65 Å radius we cal-
275 culated a charge transfer of about $0.095e^-$ to the
276 carbon from the three first nearest neighbor boron
277 atoms, with other B sites showing negligible
278 change in charge. This charge transfer also reflects
279 the stronger potential and larger electronegativity
280 of C, and provides substitutional C with definite
281 anionic character.

4. 10% Doping   282

283   We have also performed a virtual crystal calcula-
284 tion for the 10% doped $x = 0.10$ system $Mg(B_{0.9}C_{0.1})_2$.
285 The DOS and band structure are shown in Figs. 5
286 and 6. By aligning the highest peaks in the DOS at
287 -2 eV and $+6$ eV (they can be aligned simulta-
288 neously), we establish that the differences are (1)
289 an increase in the occupied bandwidth (at the
290 MgB_2 band filling) from 12.4 eV to 12.5 eV
291 ($\sim$1%), and (2) the raising of the Fermi level by
292 0.3 eV to accommodate the extra electrons. Other-
293 wise there is very little difference in the two densities
294 of states. This raising of E_F will be compared to the
295 supercell result in the next section. At this band
296 filling, the VCA gives the σ-band edge at Γ precisely
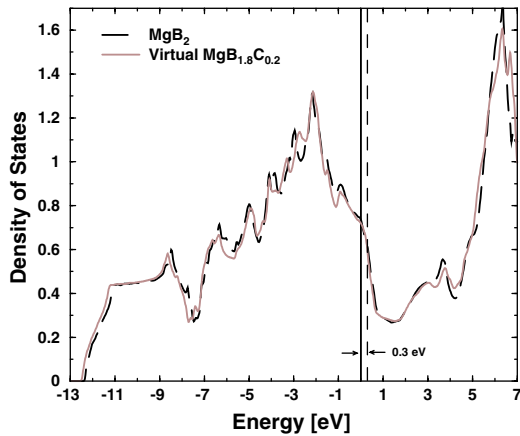
Fig. 5. Density of states of $Mg(B_{0.9}C_{0.1})_2$. The Fermi level moves up by 0.3 eV due to doping.
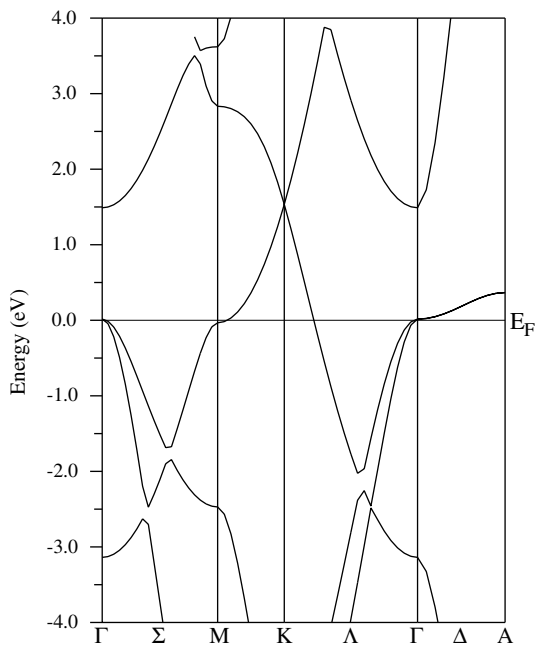
Fig. 6. Band structure of $Mg(B_{1-x}C_x)_2$, $x = 0.10$, in the virtual crystal approximation. The σ-bands at Γ lie precisely at E_F, so the Fermi cylinder radii at Γ vanish, corresponding to a topological transition.

297 at E_F as shown in Fig. 6. At the point A it is still
298 about 0.3 eV above E_F, meaning that both cylindri-
299 cal Fermi surfaces have shrunk to a point at their
300 "waists."

5. σ hole concentration   301

It is accepted that superconductivity in MgB_2 302
arises from hole-doping of the σ bonding hole   303
states due to the intrinsic chemistry [13] of   304
MgB_2. The observed decrease in electron–phonon 305
coupling strength, and hence T_c upon C addition, 306
makes the change in hole concentration one of the 307
major points of interest. We have calculated the 308
hole concentration of both the 8.33% supercell sys- 309
tem and the 10% virtual system from the volume   310
enclosed by the Fermi surface. Since the radii of 311
the cylindrical Fermi surfaces are only slightly dif- 312
ferent along the $\Gamma \to M$ and the $\Gamma \to K$ directions, 313
we calculated the average basal area by consider- 314
ing the value along the $\Gamma \to M$ direction only. 315
Also, we assumed a sinusoidal dependence of the 316
Fermi surface along the $\hat{c}$ axis, allowing analytic 317
evaluation of the Fermi surface volumes i.e. the 318
hole concentrations. The results are presented in 319
Table 2. In the process of calculating the number 320
of holes, electronic structure reveals that both the 321
σ-band Fermi surfaces are still intact, consistent 323
with the two-band superconductivity with substan- 324
tial T_c as seen in experiments [8]. Also, we interpo- 325
lated the number of holes for the 10% doped   326
system (virtual crystal) to calculate the value for 327
the 8.33% doped system. Supercell calculation   328
gave 0.070 holes/cell while the extrapolation gave 329
only 0.057 holes/cell. This indicates that the virtual 330
crystal approximation is not very reliable for sub- 331
stitutional carbon, and that C cannot be thought 332
of "boron + an electron."

6. Coherent potential approximation results   333

For further comparison and to assess the effects 334
of disorder, we have performed CPA studies of   335

Table 2
Calculated number of σ holes for the various C concentrations discussed in the text

	No. of holes (holes/cell)
MgB_2	0.11
8.33% Doping $Mg_6B_{11}C$ supercell	0.070
10% Doping $MgB_{1.8}C_{0.2}$ virtual crystal	0.0463
8.33% Doping $MgB_{1.833}C_{0.167}$ extrapolation	0.057

this system. We have carried out CPA calculations (1) at $x = 0.0001$ to provide a "perfect crystal" reference for evaluation of the various algorithms in the CPA code, (2) at $x = 0.0833$ for most direct comparison to the $x = 1/12$ (ordered) supercell calculations described in the previous sections, and (3) at $x = 0.10$ and 0.20 as representative of the system toward the upper range of achievable C substitution. The spectral function over the whole energy range of interest, plotted as a "smeared" band structure, is shown for the $x = 0.20$ case in Fig. 7. The primary points of interest are the filling of the σ-band hole states, and the broadening (and potentially splitting) of bands.

The full energy region is presented in Fig. 7 for $x = 0.20$ (where broadening is more easily seen) to illustrate the strong wavevector (k) and energy (E) dependence of the broadening of the spectral function. The largest disorder occurs in the 2s region in the lower valence band, where the C 2s state is noticeably lower in energy leading to increased smearing. The other region of large disorder is from +3 eV upward, but some states remain comparatively sharp. The flat band at 5 eV along Γ–M and A–L, with strong π character, is the lowest conduction band that is strongly affected by the disorder. The bands around the Fermi level, whether σ or π, are among those less affected by the chemical disorder. As expected from the virtual crystal results for $x = 0.10$ from the previous section, the σ-band holes are completely filled at

Fig. 7. CPA spectral density in the full valence–conduction band region, for $x = 0.20$, plotted as a broadened band structure. Disorder broadening is largest below −8 eV in the valence bands and above 4 eV in the conduction bands.

$x = 0.20$, as revealed by the flat band along the Γ–A line lying entirely below E_F. The band filling behavior versus x is quantified below.

In the valence (occupied) bands, disorder broadening is large in the lower s-band region −8 eV to −14 eV below E_F, and somewhat less so where the (primarily σ) band in the −3 to −4 eV range gets flat around the zone edge M and L points. Similar broadening does not occur in the same band at the (more distant from Γ) zone edge K and H points, where the band lies at −6 eV and is much less flat. The top of the σ bonding bands along Γ–A are comparatively sharp; the width is quantified below.

In the conduction bands disorder broadening becomes more prevalent. The antibonding σ*-bands (flat along Γ–A at +6 eV) are much broader than their bonding counterparts (below E_F), and this band along Γ–M and A–L with Mg 3s character becomes exceedingly diffuse. The π-bands show strong k-dependence of the broadening, beginning at 2–3 eV around the M point and becoming wider in the 6–10 eV range (and above, not shown in the figure).

6.1. Carbon concentration dependence

The x-dependence of the broadening can be seen in Fig. 8 for $x = 0.0001$ (the CPA equivalent of $x = 0$ MgB$_2$), for $x = 0.10$, and for $x = 0.20$ (the latter may not be experimentally accessible). Since in each case E_F is set to zero, band filling appears as downward shifts of the bands, by roughly $\delta E_F = -0.4$ eV for $x = 0.10$ and $\delta E_F = -1.0$ eV for $x = 0.20$. For $x = 0.0833$ (not shown) the σ-bands lie at the same position (with respect to E_F) as for the ordered $x = 1/12$ case shown in Fig. 3. Hence the degree of band filling in the CPA results is the same as for the ordered $x = 1/12$ case that was analyzed in the previous section. Although we will not dwell on it, it can be noticed that the band shift is not entirely rigid: the two valence bands at the L point split apart as well as broaden with increasing C concentration.

The other important aspect of the CPA bands of Fig. 8 is the broadening that increases with carbon concentration. Within the resolution of widths that we are able to extract, the widths of the σ-
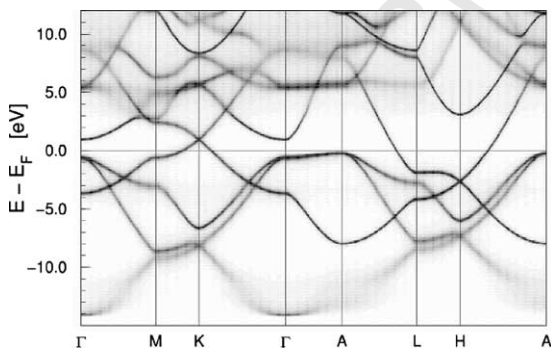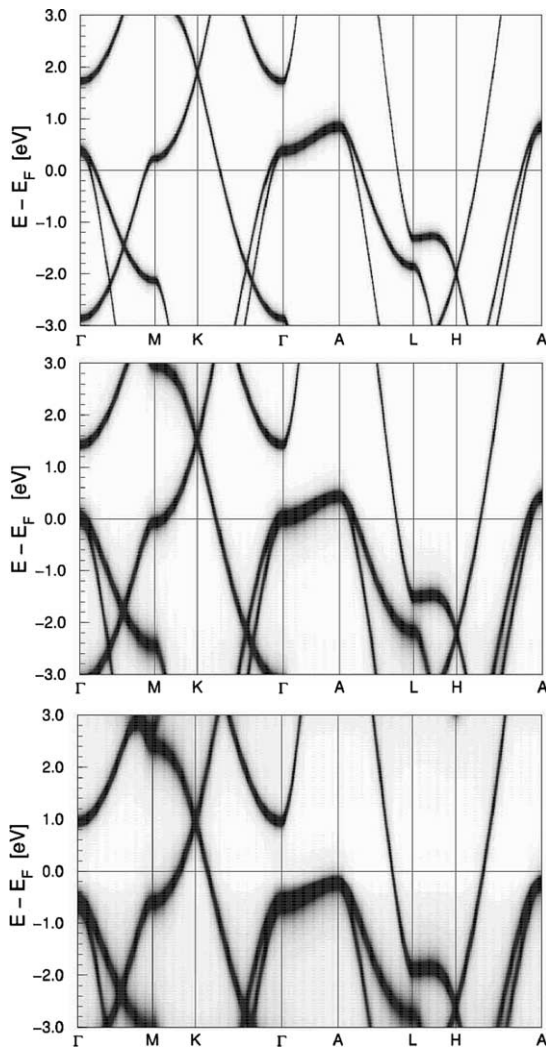
Fig. 8. CPA spectral density for $x = 0.0001$ (top panel), $x = 0.10$ (middle) and $x = 0.20$ (bottom panel). The main features are (i) the "rising" Fermi level (with respect to the σ-band along Γ–A, say), and (ii) the increase in the disorder broadening of the bands. Since the numerical algorithms cannot reproduce the δ-function bands for $x \to 0$, the $x = 0.0001$ case is included as a reference for the algorithmic contribution to the width.

413 bands can be taken to be proportional to x, but
414 differ considerably between Γ and A (being about
415 50% wider at Γ). The full width at half maximum
416 of the spectral density of the σ-bands, averaged
417 between Γ and A, is about $\gamma \approx 0.21$ eV (to perhaps
418 10% accuracy). This width corresponds to a width

419 in wavevector given by $\gamma = v_F \delta k$, and therefore a
420 mean free path of $\ell_F = 2\pi v_F/\gamma$. The 60 meV split-
421 ting of the σ-bands (see Section 3.1) for the
422 $x = 1/12$ ordered supercell implies that the
423 0.21 eV mean width can be interpreted as 0.05 eV
424 from the B/C on-site energy difference, and thus
425 0.16 eV from disorder itself.
      Due to the anisotropy of the Fermi velocity v_F,   426
427 the mean free path may vary considerably over the
428 Fermi surface at $x = 0.10$. At Γ the cylinder radius
429 has shrunk to a point, and the very small z compo-
430 nent of v_F (vanishing at Γ) suggests a very small
431 mean free path in the z direction of the order of
432 the layer spacing c for $x = 0.10$.

7. Discussion and summary   433

434 In the band structure of the 8.33% doped super-
435 cell system, the hole σ-band Fermi surfaces along
436 the $\Gamma \to A$ direction are still present, and this de-
437 gree of band filling is reproduced by the CPA.
438 Even for $x = 0.10$ the virtual crystal picture (which
439 overestimates the rate of band filling by C) leaves
9   σ Fermi surfaces, just beginning to be pinched
441 off. The CPA calculations (Fig. 8) show the σ-
442 band holes begin to disappear rapidly for $x >$
443 0.10. Qualitatively this filling is consistent with
444 most experimental reports.
445 The questions, and experimental probes, should
446 now be focused on the fact that, as the σ-band fills,
447 there will be very strong deviation from 'business
448 as usual' in the coupled electron–phonon system.
449 The strength of coupling of bond-stretching modes
450 with $Q < 2k_F$ continues to increase, and conven-
451 tional Migdal–Eliashberg theory ceases to apply.
452 The dynamics of these ultra-strongly coupled
453 modes is unexplored, with their peculiar character
454 being signaled by the divergence of their linewidth
455 (at least within Migdal–Eliashberg theory). The
456 limiting behavior should not revert to the widely
457 studied polaron limit, however, as there remain
458 the background π electrons, which are weakly cou-
459 pled to vibrations but provide full metallic conduc-
460 tivity and screening to the system. The present
461 study reveals that C substitution for B provides a
462 similarly favorable system to Al substitution for
463 Mg for studying this evolution. Recent reports

indicate that Sc substitution ($Mg_{1-x}Sc_xB_2$) may also provide [32] another such system for study.

Acknowledgements

References

[1] A. Gurevich, S. Patnaik, V. Braccini, K.H. Kim, C. Mielke, X. Song, L.D. Cooley, S.D. Bu, D.M. Kim, J.H. Choi, et al., Supercond. Sci. Technol. 17 (2004) 278.

[2] J.S. Slusky, N. Rogado, K.S. Regan, M.A. Hayward, P. Khalifah, T. He, K. Inumaru, S.M. Loureiro, M.K. Haas, H.W. Zandbergen, et al., Nature 410 (2001) 343.

[3] G. Profeta, A. Continenza, S. Massidda, Phys. Rev. B 68 (2003) 144508.

[4] V. Barabash, D. Stroud, Phys. Rev. B 66 (2002) 012509.

[5] U. Burkhardt, V. Gurin, F. Haarmann, W.S.H. Borrmann, A. Yareskko, Y. Grin, J. Solid State Chem. 177 (2004) 389.

[6] I. Maurin, S. Margadonna, K. Prassides, T. Takenobu, Y. Iwasa, A.N. Fitch, Chem. Mater. 14 (2002) 3894.

[7] A. Bharathi, S.J. Balaselvi, S. Kalavathi, G.L.N. Reddy, V.S. Sastry, Y. Hariharan, T.S. Radhakrishnan, Physica C 370 (2002) 211.

[8] H. Schmidt, K.E. Gray, D.G. Hinks, J.F. Zsadzinski, M. Avdeev, J.D. Jorgensen, J.C. Burley, Phys. Rev. B 060508 (2003) 68.

[9] M. Andeev, J.D. Jorgensen, R.A. Ribiero, S.L. Bud'ko, P.C. Canfield, Physica C 301 (2003) 387.

[10] R.A. Ribiero, S.L. Bud'ko, C. Petrovic, P.C. Canfield, Physica C 16 (2003) 385.

[11] T. Masui, S. Lee, S. Tajima, cond-mat/0312458 (2004).

[12] R.H.T. Wilke, S.L. Bud'ko, P.C. Canfield, D.K. Finnemore, R.J. Suplinskas, S.T. Hannahs, cond-mat/0312235 (2004).

[13] J.M. An, W.E. Pickett, Phys. Rev. Lett. 86 (2001) 4366.

[14] Z. Holanova, P. Szabo, P. Samuely, R.H.T. Wilke, S.L. Bud'ko, P.C. Canfield, cond-mat/0404096 (2004).

[15] P. Samuely, Z. Holanova, P. Szabo, J. Kacmarcik, R.A. Ribiero, S.L. Bud'ko, P.C. Canfield, Phys. Rev. B 68 (2003) 020505.

[16] R. Puzniak, M. Angst, A. Szewczyk, J. Jun, S.M. Kazakov, J. Karpinski, cond-mat/0404579 (2004).

[17] M. Avdeev, J.D. Jorgensen, R.A. Robeiro, S.L. Bud'ko, P.C. Canfield, Physica C 387 (2003) 301.

[18] Y. Yan, M.M. Al-Jassim, J. Appl. Phys. 92 (2002) 7687.

[19] S.C. Erwin, I.I. Mazin, Phys. Rev. B 68 (2002) 132505.

[20] P.P. Singh, cond-mat/0304436 (2003).

[21] J.M. An, H. Rosner, S.Y. Savrasov, W.E. Pickett, Physica B 328 (2003) 1.

[22] W.E. Pickett, J.M. An, H. Rosner, S.Y. Savrasov, Physica C 387 (2003) 117.

[23] Y. Kong, O.V. Dolgov, O. Jepsen, O.K. Andersen, Phys. Rev. B 64 (2001) 020501.

[24] L. Boeri, G.B. Bachelet, E. Cappelluti, L. Pietronero, Phys. Rev. B 65 (2002) 214501.

[25] W.E. Pickett, Braz. J. Phys. 33 (2003) 695.

[26] P. Blaha, K. Schwarz, G.K.H. Madsen, D. Kvasnicka, J. Luitz, J. Phys. Chem. Sol. 63 (2002) 2201.

[27] J.P. Perdew, K. Burke, M. Ernzerhof, PRL 77 (1996) 3865.

[28] E. Sjostedt, L. Nordstrom, D.J. Singh, Solid State Commun. 114 (2000) 15.

[29] K. Koepernik, H. Eschrig, Phys. Rev. B 59 (1999) 1743.

[30] K. Koepernik, B. Velicky, R. Hayn, H. Eschrig, Phys. Rev. B 55 (1997) 5717.

[31] J.A. Blackman, D.M. Esterling, N.F. Berk, Phys. Rev. B 4 (1971) 2412.

[32] S. Agrestini, C. Metallo, M. Filippi, L. Simonelli, G. Campi, C. Sanipoli, E. Liarokapis, S.D. Negri, M. Giovannini, A. Saccone, et al., cond-mat/0408095.